Eur. Phys. J. C (2017) 77:910
https://doi.org/10.1140/epjc/s10052-017-5483-4

THE EUROPEAN PHYSICAL JOURNAL C

Regular Article - Theoretical Physics

Central and peripheral interactions of hadrons

I. M. Dremin[1,2,a], **V. A. Nechitailo**[1], **S. N. White**[3]

[1] Lebedev Physics Institute, Moscow 119991, Russia
[2] National Research Nuclear University "MEPhI", Moscow 115409, Russia
[3] CERN, 1211 Geneva 23, Switzerland

Received: 20 September 2017 / Accepted: 19 December 2017 / Published online: 28 December 2017

Abstract Surprisingly enough, the ratio of elastic to inelastic cross sections of proton interactions increases with energy in the interval corresponding to ISR→LHC (i.e. from 10 to 10^4 GeV). That leads to special features of their spatial interaction region at these and higher energies. Within the framework of some phenomenological models, we show how the particular ranges of the transferred momenta measured in elastic scattering experiments expose the spatial features of the inelastic interaction region according to the unitarity condition. The difference between their predictions at higher energies is discussed. The notion of central and peripheral collisions of hadrons is treated in terms of the impact-parameter description. It is shown that the shape of the differential cross section in the diffraction cone is mostly determined by collisions with intermediate impact parameters. Elastic scattering at very small transferred momenta is sensitive to peripheral processes with large impact parameters. The role of central collisions in the formation of the diffraction cone is less significant.

1 Introduction

Traditionally, hadron collisions were classified according to our prejudices about hadron structure. From the earlier days of Yukawa's prediction of pions, the spatial extent of hadrons was ascribed in pre-QCD times to the pion cloud (of size of the inverse pion mass) surrounding their centers. The very external shell was described as formed by single virtual pions representing the lightest particle constituents. The deeper shells were occupied by heavier objects (2π, ρ-mesons etc.). In the quantum field theory, these objects contribute to hadron scattering amplitudes by their propagators polynomially damped for transferred momenta of the order of the corresponding masses. Therefore, according to the Heisenberg principle, the largest spatial extent is typical for the single-pion (smallest masses!) exchange. That is why the one-pion exchange model was first proposed [1] for the description of inelastic peripheral interactions of hadrons. Later on, more central collisions with the exchange of ρ-mesons and all other heavier Regge particles were considered and included in the multiperipheral models.

Some knowledge about the spatial extent of inelastic hadron interactions can also be gained from properties of their elastic scattering connected with inelastic processes by the unitarity condition. The spatial view of the collision process of two hadrons is not directly observable because of their extremely small sizes and its short time-duration. However, it is very important for our heuristic view. The interaction region is characterized by the impact parameter b which denotes the shortest transverse distance between the trajectories of the centers of the colliding hadrons. Different spatial regions are responsible for the relation with different ranges of the transferred momenta in the experimentally measured differential cross section.

To analyze this relation we choose the particular QCD-motivated model [2,3] which we call by the first letters of the names of its coauthors as the kfk-model. This model has described quite precisely the present experimental measurements of the elastic scattering of protons from ISR to LHC energies. The energy dependence imposed by the model is used for predictions at higher energies. We compare its conclusions with other approaches to the problem.

The kfk-model provides analytically the shapes of the elastic scattering amplitude in terms of both the transferred momenta t measured experimentally and the impact parameters b relevant for the spatial view of the process. That allows one to study separately different regions of them and their mutual influence, i.e. to reveal "the anatomy" of the model.

We consider both approaches and show:

1. How different t-regions represented by the measured differential cross section contribute to the shape of the

[a] e-mail: dremin@lpi.ru

spatial interaction region and to the unitarity condition (Sects. 5 and 6);
2. How different spatial b-regions contribute to the measurable t-structure of the elastic scattering amplitude (Sect. 7).

2 The kfk-model

The kfk-model [2,3] originates from the so-called Stochastic Vacuum Model [4,5] which was initially formulated by deriving the impact-parameter shape of the elastic scattering amplitude using some QCD-motivated arguments. Applying the Fourier–Bessel transformation one gets the elastic amplitude in terms of the transferred momenta. It has been shown [2,6] that the resulting shape describes well the data on $\mathrm{d}\sigma/\mathrm{d}t$, $\sigma_{\rm el}$, $\sigma_{\rm tot}$ at energies from ISR (11–60 GeV in the center of mass system) [7] through LHC (2.76–13 TeV) [8–14] with the help of the definite set of the energy dependent parameters.

The differential cross section is defined as

$$\mathrm{d}\sigma/\mathrm{d}t = |f(s,t)|^2 = f_I^2 + f_R^2, \tag{1}$$

where the labels $K = I, R$ denote correspondingly the imaginary and real parts of the elastic amplitude $f(s,t)$ (of the dimension GeV^{-2}). The variables s and t are the squared energy and transferred momentum of colliding protons in the center of mass system $s = 4E^2 = 4(p^2 + m^2)$, $-t = 2p^2(1-\cos\theta)$ at the scattering angle θ.

The nuclear part of the amplitude f in the kfk-model is

$$f_K(s,t) = \alpha_K(s)\mathrm{e}^{-\beta_K|t|} + \lambda_K(s)\Psi_K(\gamma_K(s),t), \tag{2}$$

with the characteristic shape function

$$\Psi_K(\gamma_K(s),t) = 2\mathrm{e}^{\gamma_K}\left[\frac{\mathrm{e}^{-\gamma_K\sqrt{1+a_0|t|}}}{\sqrt{1+a_0|t|}} - \mathrm{e}^{\gamma_K}\frac{\mathrm{e}^{-\gamma_K\sqrt{4+a_0|t|}}}{\sqrt{4+a_0|t|}}\right]. \tag{3}$$

In what follows, we use the explicit expressions for the energy dependent parameters α, β, γ, λ shown in [2] which fitted the data. In total, there are eight such parameters each of which contains the energy independent terms and those increasing with energy s as $\log\sqrt{s}$ and $\log^2\sqrt{s}$ (see Eqs. (29)–(36) in [3]). Thus eight coefficients have been determined from comparison with experiment at a given energy and 24 for the description of the energy dependence in a chosen interval. The parameter $a_0 = 1.39\,\mathrm{GeV}^{-2}$ is proclaimed to be fixed.

Let us note that we have omitted the nuclear-Coulomb interference term because of the extremely tiny region of small transferred momenta where it becomes noticeable.

The corresponding dimensionless nuclear amplitude in the b-representation is written as

$$\tilde{f}_K(s,b) = \frac{\alpha_K}{2\beta_K}\mathrm{e}^{-b^2/4\alpha_K} + \lambda_K\tilde{\Psi}_K(s,b) \tag{4}$$

with

$$\tilde{\Psi}_K(s,b) = \frac{2\mathrm{e}^{\gamma_K-\sqrt{\gamma_K^2+b^2/a_0}}}{a_0\sqrt{\gamma_K^2+b^2/a_0}}(1-\mathrm{e}^{\gamma_K-\sqrt{\gamma_K^2+b^2/a_0}}). \tag{5}$$

The two-dimensional Fourier transformation used is

$$\tilde{f}(s,b) = \frac{1}{2\pi}\int \mathrm{d}^2\mathbf{q}\mathrm{e}^{-i\mathbf{qb}}f(s,t=-q^2). \tag{6}$$

3 The unitarity condition

From the theoretical side, the most reliable (albeit rather limited) information as regards the relation between elastic and inelastic processes comes from the unitarity condition. The unitarity of the S-matrix $SS^+ = 1$ relates the amplitude of elastic scattering $f(s,t)$ to the amplitudes of inelastic processes M_n. In the s-channel they are subject to the integral relation (for more details see, e.g., [15–18]) which can be written symbolically as

$$f_I(s,t) = I_2(s,t) + g(s,t) = \int \mathrm{d}\Phi_2 f(s,t_1)f^*(s,t_2) + \sum_n \int \mathrm{d}\Phi_n M_n M_n^*. \tag{7}$$

The non-linear integral term represents the two-particle intermediate states of the incoming particles integrated over transferred momenta t_1 and t_2 combining to final t. The second term represents the shadowing contribution of inelastic processes to the imaginary part of the elastic scattering amplitude. Following [19] it is called the overlap function. This terminology is ascribed to it because the integral there defines the overlap within the corresponding phase space $\mathrm{d}\Phi_n$ between the matrix element M_n of the nth inelastic channel and its conjugated counterpart with the collision axis of initial particles deflected by an angle θ in proton elastic scattering. It is positive at $\theta = 0$ but can change sign at $\theta \neq 0$ due to the relative phases of inelastic matrix elements M_n's.

At $t = 0$ it leads to the optical theorem,

$$f_I(s,0) = \sigma_{\rm tot}/4\sqrt{\pi}, \tag{8}$$

and to the general statement that the total cross section is the sum of cross sections of elastic and inelastic processes,

$$\sigma_{\rm tot} = \sigma_{\rm el} + \sigma_{\rm inel}. \tag{9}$$

If divided by $\sigma_{\rm tot}$ this relation tells that the total probability of all processes is equal to 1.

It is possible to study the space structure of the interaction region of colliding protons using information as regards their elastic scattering within the framework of the unitarity condition. The whole procedure is simplified because in the space representation one gets an algebraic relation between the elastic and inelastic contributions to the unitarity condition in place of the more complicated non-linear integral term I_2 in Eq. (7).

In what follows we prefer to use the different notation of $\tilde{f}$ in (6) for clearer distinction from f:

$$i\Gamma(s,b) = \frac{1}{2\sqrt{\pi}} \int_0^\infty \mathrm{d}|t| f(s,t) J_0(b\sqrt{|t|}). \tag{10}$$

Applying directly the transformation (10) to the relation (7) one gets the unitarity condition in the b-representation

$$G(s,b) = 2\Gamma_R(s,b) - |\Gamma(s,b)|^2. \tag{11}$$

The left-hand side (the overlap function in the b-representation) describes the transverse impact-parameter profile of inelastic collisions of protons. It is just the Fourier–Bessel transform of the overlap function g. It satisfies the inequalities $0 \le G(s,b) \le 1$ and determines how absorptive the interaction region is, depending on the impact parameter (with larger G for larger absorption). The profile of elastic processes is determined by the subtrahend in Eq. (11). Thus Eq. (11) establishes the relation between the elastic and inelastic impact-parameter distributions $G(s,b) = \mathrm{d}^2\sigma_{\rm inel}/\mathrm{d}b^2$ and $|\Gamma(s,b)|^2 = \mathrm{d}^2\sigma_{\rm el}/\mathrm{d}b^2$ with $2\Gamma_R(s,b) = \mathrm{d}^2\sigma_{\rm tot}/\mathrm{d}b^2$.

If $G(s,b)$ is integrated over all impact parameters, it leads to the cross section for inelastic processes. The terms on the right-hand side would produce the total cross section and the elastic cross section, correspondingly, as should be the case according to Eq. (9). The overlap function is often discussed in relation with the opacity (or the eikonal phase) $\Omega(s,b)$ such that $G(s,b) = 1 - \exp(-\Omega(s,b))$. Thus, larger absorption corresponds to larger Ω.

4 Brief review of the elastic scattering data

Equation (11) shows that the inelastic profile G is directly expressed in terms of the elastic amplitude. Therefore let us describe experimentally measured properties of elastic scattering and discuss how they are reproduced by the kfk-model.

The bulk features of the differential cross section at high energies with increase of the transferred momentum $|t|$ can be briefly stated as its fast decrease at low transferred momenta within the diffraction cone and somewhat slower decrease at larger momenta. The diffraction cone is usually approximated by the exponent $\exp(B(s)t)$ while further decrease in the so-called Orear region is roughly fitted by a smaller than B slope or by the dependence of the type $\exp(-c\sqrt{|t|})$. For the recent data at 13 TeV see [20].

There are some special features to be noted. The increase towards $t = 0$ in the very tiny region of extremely low momenta becomes steeper. That is ascribed to the interference of nuclear and Coulomb amplitudes. It serves to determine the ratio of the real and imaginary parts of the amplitude $\rho = f_R/f_I$ at $t = 0$. In the transition region between the two main regimes the differential cross section flattens somewhat and/or shows some dip. It will be specially discussed below. At transferred momenta larger than those of the Orear region further flattening is observed. This tail is usually described perturbatively by the three-gluon exchange with real amplitude. However, the cross section is so small there that this region is unimportant for our conclusions.

The optical theorem (8) ensures us that the imaginary part of the amplitude in forward direction must be positive at all energies. The real part at $t = 0$ has been measured also to be positive at high energies and comparatively small ($\rho \approx 0.1 - 0.14$). For recent data at 13 TeV see [21]. This result agrees with predictions of the dispersion relations. Thus it only contributes about 1 or 2% to the forward differential cross section (1).

In principle, both real and imaginary parts can be as positive as negative at other transferred momenta. Anyway, they are bounded by the values $\pm\sqrt{\mathrm{d}\sigma/\mathrm{d}t}$ and must be small in those t-regions where the differential cross section is small. Actually, these two bounds are used for two different approaches considered below. They determine the difference between their predictions about the shape of the interaction region.

The further knowledge about the elastic amplitudes comes either from some theoretical considerations or from general guesses and the model building. It was shown in Refs. [22,23] that the real part of the amplitude must change its sign somewhere in the diffraction cone. Therefore, its decrease with increasing $|t|$ inside the diffraction cone must be faster than that of the imaginary part which then should mainly determine the value of the slope $B(s)$. The dip between the two main typical regimes of the diffraction cone and Orear behavior inspires the speculation that the imaginary part also passes through zero near the dip. Then the dip of the differential cross section is filled in by the small real part of the amplitude. These guesses are well supported by the results of the kfk-model used by us.

5 How different t-regions contribute to the b-shape of the interaction region

At the outset we will not discuss the spatial extension of the interaction region as a function of the impact parameter b. It was carefully studied in several publications [7,24–28]. Instead, we limit ourselves by the simpler case of the energy dependence of the intensity of interaction for central (head-on) collisions of impinging protons at $b = 0$. That is the most sensitive point of the whole picture demonstrating its crucial features.

Let us introduce the variable ζ:

$$\zeta(s) = \Gamma_R(s,0) = \frac{1}{2\sqrt{\pi}} \int_0^\infty \mathrm{d}|t| f_I(s,t). \tag{12}$$

To compute the integral, one must know the behavior of the imaginary part of the amplitude for all transferred momenta t at a given energy s. The choice of the sign of f_I at large $|t|$ is important for model conclusions.

Now, have a look at the second term in the unitarity condition (11):

$$|\Gamma(s,0)|^2 = \zeta^2 + \frac{1}{4\pi}\left(\int_0^\infty \mathrm{d}|t| f_R(s,t)\right)^2. \tag{13}$$

The last term here can be neglected compared to the first one. That is easily seen from the inequalities

$$2\sqrt{\pi}\Gamma_I(s,0) = \int_0^\infty \mathrm{d}|t| f_R \le \int_0^\infty \mathrm{d}|t||f_R| = \int_0^\infty \mathrm{d}|t| \sqrt{\frac{\rho^2(s,t)\mathrm{d}\sigma/\mathrm{d}t}{1+\rho^2(s,t)}} \ll 2\sqrt{\pi}\zeta. \tag{14}$$

Here $\rho(s,t) = f_R(s,t)/f_I(s,t)$. The factor $\rho^2(s,t)/(1+\rho^2(s,t))$ is very small in the diffraction cone because $\rho^2(s,0) \le 0.02$ according to experimental results and $\rho(s,t)$ should possess zero inside the diffraction cone [22,23]. It can become of the order 1 at large values of $\rho^2(s,t)$ (say, at the dip) but the cross section $\mathrm{d}\sigma/\mathrm{d}t$ is small there already [8,29]. The smallness of the contribution from the real part to $|\Gamma|^2$ is strongly supported by the kfk-model as shown in Table 1 below.

Then the unitarity condition (11) for central collisions can be written as

$$G(s, b=0) = \zeta(s)(2-\zeta(s)). \tag{15}$$

Thus, according to the unitarity condition (15) the darkness $G(s,0)$ of the inelastic interaction region for central collisions (absorption) is defined by the single energy dependent parameter $\zeta(s)$. It has the maximum $G(s,0) = 1$ for $\zeta = 1$. Any decline of ζ from 1 ($\zeta = 1 \pm \epsilon$) results in the parabolic decrease of the absorption ($G(s,0) = 1-\epsilon^2$), i.e. in an even much smaller decline from 1 for small ϵ. The elastic profile, equal to ζ^2 in central collisions, also reaches the value 1 for $\zeta = 1$. Namely the point $b = 0$ happens to be most sensitive to the variations of ζ in different models.

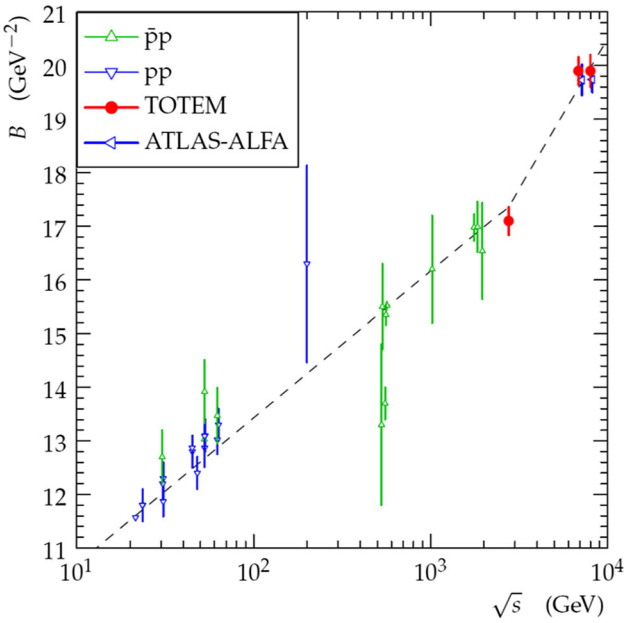

Fig. 1 The experimental data about the diffraction cone slope $B(s)$ [30]

Formally, the unitarity condition (15) imposes the limit $\zeta \le 2$. It is required by the positivity of the inelastic profile. This limit corresponds to the widely discussed "black disk" picture which requires the relation

$$\sigma_{\mathrm{el}} = \sigma_{\mathrm{inel}} = \sigma_{\mathrm{tot}}/2. \tag{16}$$

Both real and imaginary parts of the amplitude are analytically prescribed by the kfk-model. That allows one to calculate the experimental characteristics and get direct insight into the validity of some approximations. Figure 1 reproduces the experimental data about the diffraction cone slope $B(s)$ [30] and Fig. 2 demonstrates how they are fitted by the kfk-model from ISR to LHC energies. The fit is good in general but one sees some discrepancy at low ISR energies and at TOTEM 2.76 TeV data.

In Table 1 we show the energy dependence of several characteristics of proton collisions with estimates of the role of different regions of integration in (12) when computed according to the prescriptions for f_I and f_R of the kfk-model. This "anatomy" answers the question raised at the title of the section.

The exact value of $\zeta(s)$ is crucial for our conclusions, especially if ζ closely approaches 1 as occurs at LHC energies. Its values in the kfk-model at energies from 7 to 10^4 TeV are shown in first line of Table 1. They approach 1 asymptotically

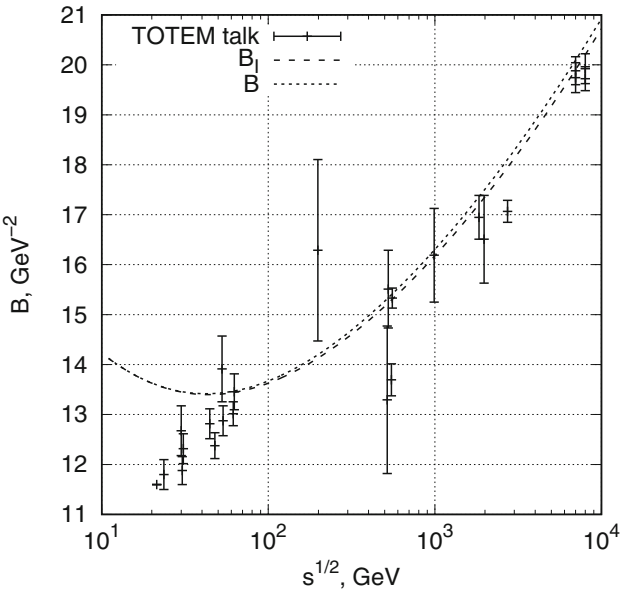

Fig. 2 The fit of the B-data (Fig. 1) by the kfk-model (the dotted line). The dashed line B_I indicates that the slope is well accounted by the imaginary part of the amplitude alone

Table 1 The energy behavior of main pp-characteristics of the kfk-model (their detailed explanation is given in the text)

$\sqrt{s}$, TeV	7	100	10^4
ζ	0.95058	0.99531	0.99793
$\lvert t_0\rvert$,GeV^2	0.47566	0.28458	0.13978
$\zeta[0, \lvert t_0\rvert]$	0.99193	1.0769	1.1505
$\zeta[\lvert t_0\rvert, \infty]$	−0.041349	−0.081548	−0.15260
$G(s, 0)$	0.99756	0.99998	1.00000
$\Gamma_I[0, \lvert t_0\rvert]$	0.053928	0.054432	0.047289
$\Gamma_I[\lvert t_0\rvert, \infty]$	0.003405	0.001024	−0.001311
Γ_I^2	0.003287	0.003075	0.002114
$4\sigma_{\rm el}/\sigma_{\rm tot}$	1.03	1.148	1.26
$\sigma_{\rm inel}/\sigma_{\rm el}$	2.89	2.48	2.17
$B\lvert t_0\rvert$	9.4676	7.6956	6.2829
$\zeta(\sigma)$	1.0333	1.1584	1.3031

from below. The integrand f_I in Eq. (12) changes sign for the kfk-model as demonstrated at 7 and 10^4 TeV in Fig. 3. The energy dependence of its zeros $t = t_0(s)$ has been computed and shown in Table 1. The contributions to ζ from the positive and negative branches of the integrand are also shown there as $\zeta[0, |t_0|]$ and $\zeta[|t_0|, \infty]$. The first of them exceeds 1 at high energies and would deplete the inelastic profile at the center if not compensated by the second one. The numerical contribution of the negative tail is very small but it is decisive for the asymptotic behavior of ζ which approaches 1 and does not exceed it. Thus the central profile saturates with $G(s, 0)$ tending to 1 (see line 5 of Table 1). The whole profile becomes more Black, Edgier and Larger (the BEL-

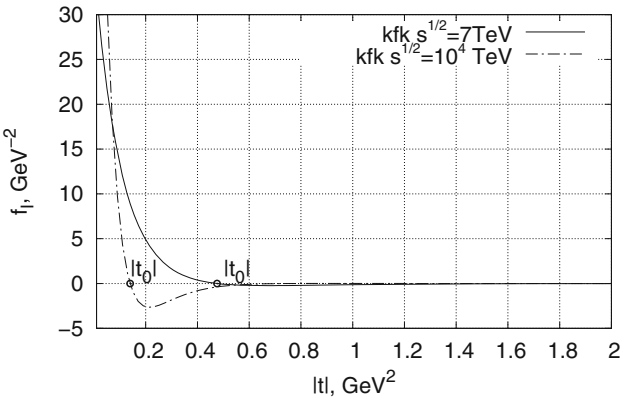

Fig. 3 The t-dependence of f_I at 7 and at 10^4 TeV (the kfk-model). The positions of zeros are shown

regime [31]) similar to the tendency observed from ISR to LHC energies (see Fig. 7 in [3]). Nothing drastic happens in the asymptotic sense!

The share of elastic processes and their ratio to inelastic collisions computed according to the kfk-model are also shown in the Table 1 (lines 9 and 10). Let us stress again that in the kfk-model the ratio $r = 4\sigma_{\rm el}/\sigma_{\rm tot}$ becomes larger than 1 with increasing energy (line 9) while ζ saturates at 1 as shown in Table 1 (line 1). This difference is crucial for asymptotic predictions about the shape of the interaction region.

To support our assumption that the real part can be neglected according to estimates of Eq. (14), we have directly computed $\Gamma_I[0, |t_0|] = \int_0^{|t_0|} d|t| f_R(s, t)/2\sqrt{\pi}$ and $\Gamma_I[|t_0|, \infty] = \int_{|t_0|}^{\infty} d|t| f_R(s, t)/2\sqrt{\pi}$ for the kfk-model. In accordance with Eq. (14) they happen to be negligibly small as seen from Table 1 at $\Gamma_I[...]$- and Γ_I^2-lines.

It is interesting to note, that, according to the kfk-model, the contribution of the imaginary part to the differential cross section dominates almost everywhere except the very narrow region near the dip (see Fig. 3 in [3]). This is also true at those transferred momenta where f_I becomes negative. Surely, the real part dominates in the narrow dip region of the differential cross section near t_0 but its integral contribution to $|\Gamma|^2$ can be neglected (compare line 1 and line 8 of Table 1).

We do not consider in detail the whole impact-parameter shape of the interaction region here because, for our purposes, it was enough to consider it at the most sensitive point of central collisions at $b = 0$. Moreover, it has been done in Refs. [7,24–28].

6 Comparison to some other models

There is no shortage of models of elastic scattering on the market nowadays. We want just to stress that the kfk-model

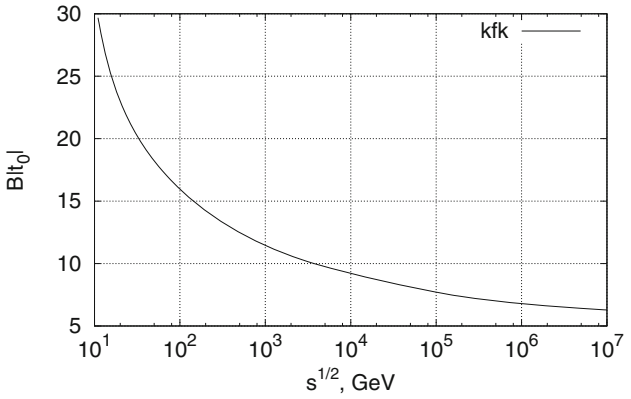

Fig. 4 The value of $B|t_0|$ decreases with energy (the kfk-model)

provides explicit analytical expressions for the amplitude both in transferred momenta and in impact parameters.

The t-behavior of their amplitude was compared by the authors with the predictions of the BSW-model [32] in Refs [2,3] and with Selyugin-model [33] in Ref. [3] at energies 7 and 14 TeV. In the measured interval of the transferred momenta they almost coincide within the experimental uncertainties. The results of the models are slightly different in the shapes at larger transferred momenta due to the different number of predicted zeros of the amplitude and can be compared with newly measured data [20,21].

The two most important features of the experimental data are well reproduced by the kfk-model. Those are the slope of the diffraction cone and the dip position which coincides practically with the zero of the imaginary part of the amplitude. Therefore, to get the easier insight, one can oversimplify the model leaving only these two parameters [34] and writing $f_I \propto (1-(t/t_0)^2)\exp(Bt/2)$ with the slope $B=(B_I+\rho^2 B_R)/(1+\rho^2)\approx B_I$. This toy-model allows one to calculate analytically the relation between r and ζ:

$$\frac{r}{\zeta}=\frac{1-\frac{4}{(Bt_0)^2}+\frac{24}{(Bt_0)^4}}{1-\frac{8}{(Bt_0)^2}}\approx 1+\frac{4}{(Bt_0)^2}+\frac{88}{(Bt_0)^4}>1. \quad (17)$$

The value of r is always larger than ζ. It exceeds ζ by about 5% at 7 TeV. It is important that their ratio (17) depends on a single quite large parameter Bt_0. The dip near t_0 shifts (see Table 1) at higher energies inside the region which at low energies traditionally belonged to the diffraction cone at $|t|<0.4$ GeV^2. The excess of r over ζ becomes larger at higher energies because $(Bt_0)^2$ decreases as seen from Table 1 and Fig. 4. It can be used as a guide in comparing further results at higher energies.

Measuring the differential cross section, we get no information about the signs of real and imaginary parts of the amplitude. The kfk-model predicts that the imaginary part changes its sign near the dip of the differential cross section. In principle, one can imagine another possibility to fit the differential cross section ascribing positive $f_I(s,t)\propto+\sqrt{\mathrm{d}\sigma/\mathrm{d}t}$, i.e. considering the positive tail of f_I. Unfortunately, it lacks any explanation of the dip in the differential cross section as a zero of the imaginary part. This assumption was used in papers [7,24–28]. Since the kfk-model claims to describe the tail of the differential cross section quite well, the proposal of positive f_I would mean that one should just subtract $\zeta[|t_0|,\infty]$ from $\zeta[0,|t_0|]$. The result is shown at the line $\zeta(\sigma)$. One concludes that, for the case of the positive tail of the imaginary part, ζ in the unitarity condition (7) can be well approximated by r shown in Table 1. The asymptotic predictions drastically change if ζ increases at higher than LHC energies and exceeds 1. The darkness of central collisions diminishes, the maximum absorption ($G=1$) moves to more peripheral values of the impact parameters b, and the interaction region looks like a toroid (see the figure in [25–27]).

One reaches similar conclusions if just the exponential fit of the diffraction cone is used where the tail of f_I is also positive but lower than for the $+\sqrt{\mathrm{d}\sigma/\mathrm{d}t}$-case. The predicted increase of ζ is somewhat slower than in the previous case but the asymptotic depletion of the inelastic profile at $b=0$ is confirmed.

At present energies the values of ζ and r differ by about 5%. Thus, the quadratically small decline of $G(s,0)$ from 1 claimed in [28] cannot be noticed within the accuracy of experimental data. The choice between different possibilities could be done if the drastic change of the exponential shape of the diffraction cone at higher energies will be observed at higher energies. Some guide to that is provided in the kfk-model by the rapid motion of the positions of zeros to smaller values of $|t_0|$ inside the former cone region with energy increase as seen from Table 1 and from the simplified treatment [34]. It is interesting to note that a slight decline from the exponentially falling t-shape of the diffraction peak was shown by the extremely precise data of the TOTEM collaboration [10] already at 8 TeV. Is that the very first signature or can be trivially explained as a combination of two different slopes for real and imaginary parts in the kfk-model?

It was proposed [35] to explain this decline as an effect of t-channel unitarity with the pion loop inserted in the Pomeron exchange graph. The s-channel "Cutkosky cut" of such a graph (its imaginary part) reproduces exactly the inelastic one-pion exchange graph first considered in [1]. Thus the external one-pion shell ascribed to inelastic peripheral interactions almost 60 years ago becomes observable at small t of the elastic amplitude at 8 TeV.

Moreover, the energy behavior of the slope $B(s)$ looks somewhat different from the logarithmic one prescribed to it by the Regge-poles. The transition between 2.76 and 8 TeV data would ask for steeper dependence (see Fig. 1) and, therefore, for a non-pole nature of the Pomeron singularity.

7 How different *b*-regions contribute to the *t*-structure of the elastic amplitude

Here we can only rely on the kfk-model where the analytical expression for the amplitude in the b-representation (4) is written. We demonstrate the evolution with energy increase of the imaginary part of the amplitude as a function of the transferred momentum in Fig. 5 for the presently available energy 7 TeV (upper part) and for "asymptotically" high energy 10^4 TeV (lower part) by the dash-dotted lines. It is clearly seen that the diffraction cone becomes much steeper and the zero moves to smaller transferred momenta at higher energies.

To reveal the substructure, the contributions from different intervals of the impact parameter are also shown. We integrate over the three different regions of the impact parameters. They are quite naturally dictated by the b-space shape of the amplitude (4). The region of small impact parameters is up to values of $b \leq 2.5\ \text{GeV}^{-1} \approx 0.5$ fm. Here the exponential term is at least twice higher than Ψ_K (see Fig. 7b in [2]). Its contribution to f_I is shown by the solid line in Figure 5. The region of large impact parameters (dotted line) is considered at distances above 1 fm. The intermediate region (dashed line) lies in between them (2.5–6 GeV^{-1}).

The most intriguing pattern is formed inside the diffraction cone. The intermediate region of impact parameters b (2.5–6 GeV^{-1}) contributes mainly there (especially for $0.15 < |t| < 0.4\ \text{GeV}^2$) at 7 TeV. However, quite sizable contributions appear from small impact parameters at $0.07 < |t| < 0.15\,\text{GeV}^2$ and, especially, from large impact parameters at very small $|t| < 0.07\,\text{GeV}^2$.

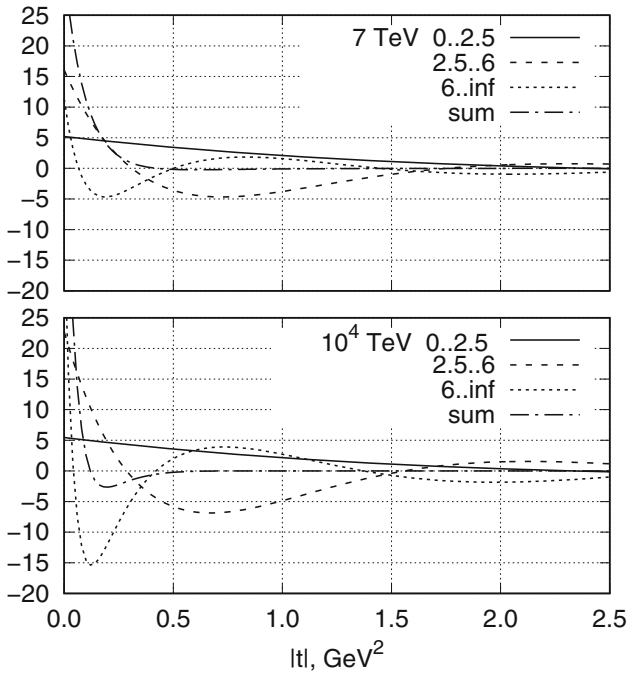

Fig. 5 The shapes of the imaginary part as a function of the transferred momentum at 7 TeV (up) and 10^4 TeV (below) are shown by the dash-dotted lines. The contributions to them from different impact parameters are also shown

At 10^4 TeV the peripheral region of large impact parameters strongly dominates at very small $|t|$ while the role of central interactions is diminished.

The remarkable feature of the kfk-model, its zero of f_I, appears due to compensations from small and medium impact parameters at 7 TeV for $|t| \approx 0.5\ \text{GeV}^2$. The peripheral region does not play an important role in its existence. In contrast to it, namely peripheral contribution is crucial at 10^4 TeV. It is compensated by the sum from the intermediate and central regions of the impact parameters at $|t| \approx 0.1\,\text{GeV}^2$.

At larger $|t|$ the damped oscillatory pattern of contributions from intermediate and peripheral regions of b dominates at all energies while the steadily decreasing (with $|t|$) share of central interactions is rather unimportant.

Let us remark that some special features of the elastic amplitude as a function of the impact parameters were discussed in [36]. In the framework of the holographic approach, it was speculated that they can be ascribed at intermediate values of b to the exchange by the black hole tubes (BH) and at larger b to the string holes (SH) (see Fig. 4 in [36]). It is tempting to relate it to the substructure seen in Fig. 5. Namely these two regions contribute mainly to the diffraction cone at 7 TeV while lower impact parameters provide slowly changing background. Thus SH-tubes are in charge of the peripheral processes and therefore have larger sizes than BH. The steep behavior of the peripheral contribution at very low transferred momenta can lead to the non-exponential curvature of the diffraction cone noticed in experiment already at 8 TeV [10,12] and interpreted as a direct impact of the long-range one-pion exchange forces (see [35]). The role of peripheral processes (i.e. the long SH-tubes) increases with energy according to Fig. 5.

8 Conclusions

Elastic scattering of protons continues to surprise us through new experimental findings. The implications of the peculiar shape of the differential cross section and the increase of the ratio of the elastic to total cross sections with increasing energy are discussed above. These facts determine the spatial interaction region of protons. Its shape can be found from the unitarity condition within definite assumptions about the behavior of the elastic scattering amplitude. The inelastic interaction region becomes more Black, Edgier and Larger (BEL) in the energy range from ISR to LHC. Its further fate at higher energies is especially interesting.

There are two possibilities discussed in the paper. The previous tendency is conserved within the kfk-model. However,

the shape of the inelastic interaction region can evolve to the so-called TEH (Toroidal Elastic Hollow) regime with more gray region of central collisions. The sign of the imaginary part of the amplitude at rather large transferred momenta is responsible for the difference between these two possibilities. It is negative in the kfk-model and positive for a different prescription. That cannot be found from present-day experiments and asks for phenomenological models. Probably, experiments with polarized protons scattered at rather large angles of the Orear region can help. The energy behavior of the ratio of elastic to total cross sections plays a crucial role. If observed, its rapid increase at higher energies would give some arguments in favor of the second possibility.

More surprises could be in store for us from the evolution of the shape of the diffraction cone with the dip position moving to smaller transverse momenta and a drastic change of its slope as shown above. First signatures of the shape evolution can be guessed even at present energies from TOTEM-findings at 2.76 and 8 TeV.

Acknowledgements I.D. is grateful for support by the RAS-CERN program and the Competitiveness Program of NRNU "MEPhI" (M.H.U.).

Funded by SCOAP[3].

References

1. I.M. Dremin, D.S. Chernavsky, JETP **38**, 229 (1960)
2. A.K. Kohara, E. Ferreira, T. Kodama, Eur. Phys. J. C **73**, 2326 (2013)
3. A.K. Kohara, E. Ferreira, T. Kodama, Eur. Phys. J. C **74**, 3175 (2014)
4. H.G. Dosch, Phys. Lett. B **199**, 177 (1987)
5. H.G. Dosch, E. Ferreira, A. Kramer, Phys. Rev. D **50**, 1992 (1994)
6. E. Ferreira, F. Pereira, Phys. Rev. D **61**, 077507 (2000)
7. U. Amaldi, K.R. Schubert, Nucl. Phys. B **166**, 301 (1980)
8. G. Antchev et al. [TOTEM Collaboration], Europhys. Lett. **96**(2), 21002 (2011)
9. G. Antchev et al. [TOTEM Collaboration], Europhys. Lett. **101**, 21002 (2013)
10. G. Antchev et al. [TOTEM Collaboration], Nucl. Phys. B **899**, 527 (2015)
11. G. Antchev et al. [TOTEM Collaboration], Eur. Phys. J. C **76**, 661 (2016)
12. T. Csörgö (for the TOTEM Collaboration). e-print arXiv:1602.00219
13. G. Aad et al. [ATLAS Collaboration], Nucl. Phys. B **889**, 486 (2014)
14. M. Aaboud et al., ATLAS Collaboration. Phys. Lett. B **761**, 158 (2016)
15. PDG group, China Phys. C **38**, 090513 (2014)
16. I.M. Dremin, Physics-Uspekhi **56**, 3 (2013)
17. I.M. Dremin, Physics-Uspekhi **58**, 61 (2015)
18. I.M. Dremin, Physics-Uspekhi **60**, 362 (2017)
19. L. Van Hove, Nuovo Cimento **28**, 798 (1963)
20. T. Csörgö [TOTEM Collaboration]. Low-x 17 conf., Bisceglie, (2017)
21. S. Giani. TOTEM Experiment Report, CERN-PRB-2017-114, 24 October (2017)
22. A. Martin, Lett. Nuovo Cimento **7**, 811 (1973)
23. A. Martin, Phys. Lett. B **404**, 137 (1997)
24. I.M. Dremin, V.A. Nechitailo, Nucl. Phys. A **916**, 241 (2013)
25. I.M. Dremin, Int. J. Mod. Phys. A **31**, 1650107 (2016)
26. I.M. Dremin, S.N. White. The interaction region of high energy protons. e-print arXiv:1604.03469
27. S.N. White. Talk at the conference QCD at Cosmic Energies, Chalkida, Greece, May 2016. http://www.lpthe.jussieu.fr/cosmic2016/TALKS/White.pdf. Accessed 2016
28. A. Alkin, E. Martynov, O. Kovalenko, S.M. Troshin, Phys. Rev. D **89**, 091501(R) (2014)
29. I.V. Andreev, I.M. Dremin, JETP Lett. **6**, 262 (1967)
30. S. Giani. TOTEM Experiment Report, CERN-PRB-2017-043, 25 April (2017)
31. R. Henzi, P. Valin, Phys. Lett. B **132**, 443 (1983)
32. C. Bourrely, J.M. Myers, J. Soffer, T.T. Wu, Phys. Rev. D **85**, 096009 (2012)
33. O.V. Selyugin, Eur. Phys. J. C **72**, 2073 (2012)
34. I.M. Dremin, Int. J. Mod. Phys. A **32**, 1750073 (2017)
35. L. Jenkovszky, I. Szanyi, Mod. Phys. Lett. A **32**, 1750116 (2017)
36. E.V. Shuryak, I. Zahed, Phys. Rev. D **89**, 094001 (2014)